Mathematical Calibration of Modular Plastic Scintillators for Various Assay Applications – 17322

James Zickefoose*, Frazier Bronson*, Henrik Jaderstrom* and Babatunde Oginni*
*Mirion Technologies (Canberra)

ABSTRACT

Plastic scintillators provide an inexpensive option to assay and characterize radioactive material. Due to the low cost it is generally possible to an array of large numbers of plastic scintillators to achieve high measurement efficiencies. The beta only thin plastic scintillators used in the Argos contamination monitors provide a convenient and reliable scintillator package that can be grouped together to form an assay system. Mathematical calibrations, using MCNP, have been produced for this detector that allow for rapid construction of various custom measurement geometries. The calibrations were constructed by comparing a series of measurements made with a number of beta and beta/gamma emitting nuclides. Characterization of the beta scintillators utilized beta emitting nuclides that included spectra from low average energy, e.g. C-14, to relatively high average energy, e.g. Sr/Y-90. In order to perform the calibration, custom versions of the standard Argos scintillators were produced that provide an MCA output for spectroscopic investigation. The spectra were then compared to detailed MCNP models in an iterative process to energy calibrate and efficiency calibrate each detector type. The validated models and energy calibrations were then tested against a number of volumetric geometries to confirm that the model would translate well to any other geometry. These validated models can then be used to rapidly construct custom measurement geometries for material measurement and screening. Two examples of measurement applications include a beta screening system for dirt on a conveyor belt and a flow through beta liquid assay system. The mathematical calibration process, validation results, and a number of application examples are discussed.

INTRODUCTION

Plastic scintillators provide a low cost means to monitor various levels of radioactive material. Unfortunately the characteristics of plastic scintillators are such that energy information about the collected radiation is in general not available. This issue is complicated when beta radiation is investigated as beta emission occurs at a continuum of energies and does not offer peaks to identify nuclides. The combination of poor energy resolution and absence of peaks makes it difficult to energy calibrate a plastic scintillator spectrum, which is necessary to properly benchmark a Monte Carlo model against a measurement. Previous works [1, 2, 3, 4] have investigated the proper energy broadening suitable to accurately describe the energy resolution of plastic scintillators. One issue arises in that the full energy collection is very poor in plastics [5], which results in the absence of full energy peaks, even when they are available in the emission spectrum, to accurately define the energy resolution of the detector.

Although energy information is limited for benchmark, it is possible to compare MCA spectra of beta emitters taken with plastic scintillators with mathematical models to determine at what energy certain features of the spectrum are expected. An example of a Cl-36 emission spectrum and a Cl-36 MCNP pulse height spectrum are shown in Figure 1. Note that the MCNP pulse height spectrum has a peak while the emission spectrum shows the absence of any peak. The pulse height spectrum peak is formed because most Cl-36 betas have sufficient energy to travel completely through the thin plastic scintillator and depositing only a fraction of their energy in the scintillation material. Due to the relatively flat stopping power of betas in the scintillator material, all betas traveling through the detector deposit very similar amounts of energy. This in turn forms a peak at low energies in the pulse height spectrum even though it is not evident in the emission spectrum. This effect can be accounted for with a proper mathematical model of the detector and source. Comparing the general shape of measured and modeled spectra along with the specific points at which the peak is formed allows for an energy calibration method for plastic scintillators.

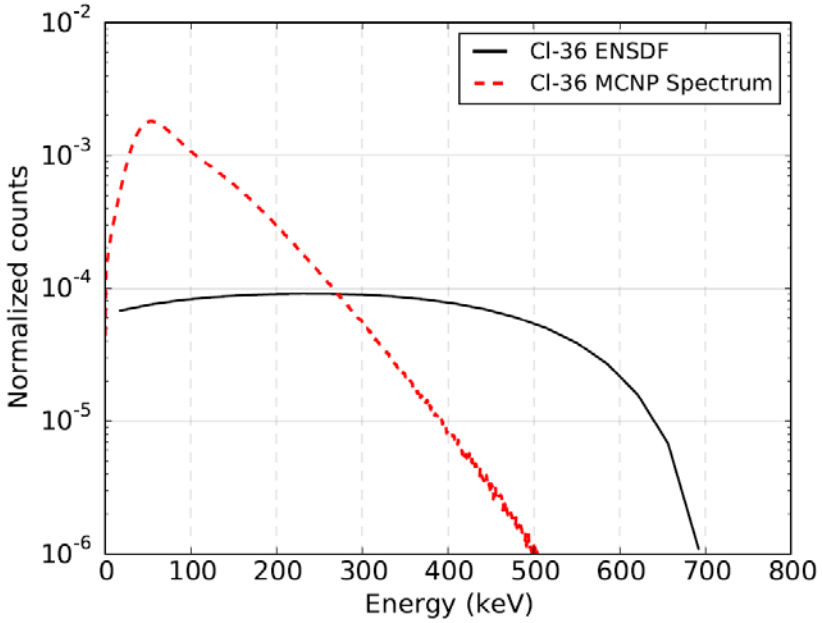

Fig. 1. Comparison of the ENSDF beta emission spectrum and a simulated pulse height detector spectrum for Cl-36. Note that the MCNP spectrum accentuates a peak at low energy.

METHODS

Monte Carlo Modeling

Monte Carlo modeling with MCNP (Monte Carlo N-Particle) [6] code is an integral part of performing an energy calibration of the scintillation detector and, once benchmarked, is the cornerstone of predicting the performance of future monitors. The modeling was conducted using MCNP-CP [7] which allows the user to model

entire beta decay continua directly from the ENSDF (Evaluated Nuclear Structure Data File) for a particular nuclide. The MCNP models also contain detailed structural information including the scintillator, dead layer, Mylar window, support/frame structures, the light pipe, and the PMT. The parameters associated with these dimensions were fine tuned in accordance with the detector drawings, but also adjusted to match geometrically simple measurements (point sources at the surface of the detector). During the MCNP simulations the energy deposition was recorded using the F8 tally and stored as a function of energy in 1 keV bins. Transport for both photons and electrons was turned on during these simulations as photons may be produced through Bremsstrahlung radiation. Furthermore, the Gaussian Energy Broadening (GEB) feature was used in the MCNP model to fully simulate the realized detector response. GEB artificially alters the energy resolution of the MCNP pulse height spectrum such that it may match that of the actual detector. Significant work has been accomplished by [1] and the GEB values recommended in that work have been adopted here.

The MCNP model was first created and benchmarked for a point source at the surface of the detector. Once appropriate confidence was achieved in the very simple model, it was extended to a point source at a distance, a surface source at the surface of the detector, a surface source a distance from the detector, and finally a surface source at a distance with various absorbers between the source and the detector. Finally, the model was applied to a source of extended thickness and benchmarked against an integral of many surface source measurements with varying thickness of absorber material between the detector and the source. Once the MCNP model is benchmarked in these various geometries it is then possible to extend the model to virtually any geometry with a reasonable confidence level. These models can then be used to determine the performance of a system long before a prototype is constructed.

Measurements

The measurements were conducted with Canberra TPS-B thin plastic scintillators, Figure 2, that are typically used in Argos contamination monitors. The active area of the detectors measures 18 cm by 36 cm and the scintillator is approximately 0.15 mm thick. The scintillator is coupled to a Lucite light pipe coupled to an embedded Electron Tubes PMT. The scintillator material is covered with an aluminized Mylar coating and protected by a honeycomb plastic frame. An on board preamplifier/amplifier processes PMT signals for analysis. A standard TPS-B detector outputs TTL pulses to the supervisory computer where they are counted and reported. In this mode the data are analyzed as gross counts with a static LLD and no energy information available. However, the detectors tested here were equipped with MCA outputs that provide an analog pulse proportional to the energy deposited in the beta scintillator. The MCA signals were fed into a Lynx MCA where data was acquired using Prospect software. The MCA signal provides all the energy information necessary to properly compare and benchmark the MCNP model against a measurement for both spectral shape and absolute efficiency.

Fig. 2. Image of the TPS-B detector. The pen is shown for scale.

Energy calibration of the MCA spectra was accomplished through a comparison with MCNP models. A number of nuclides were both measured and modeled in highly reproducible geometries where all materials in the vicinity of the measurement were known to a high degree. Measurements were compared directly to MCNP modeled spectra to determine the points at which the number of counts in the spectrum reached a maximum, where it dropped to 1/10 the maximum, and where it dropped to 1/100 the maximum. An example of these points is seen in Figure 3A for the MCNP spectrum of Sr/Y-90. The process of the energy calibration hinges on obtaining the energy information for these various points of the spectrum from the MCNP model and the channel information for these same points from the measurement. With the corresponding energy and channel information for each of the points (peak, peak/10, and peak/100) an energy calibration can be determined by producing a linear fit. In order to improve the energy calibration the three energy calibration data points were obtained for C-14, Tc-99, Cs-137, Cl-36, and Sr/Y-90 spectra. The line of best fit through these data, see Figure 3B, provide the energy calibration for the detector. Once energy calibrations were performed, the measured and modeled spectra were compared across all nuclides for both spectrum shape and absolute efficiency.

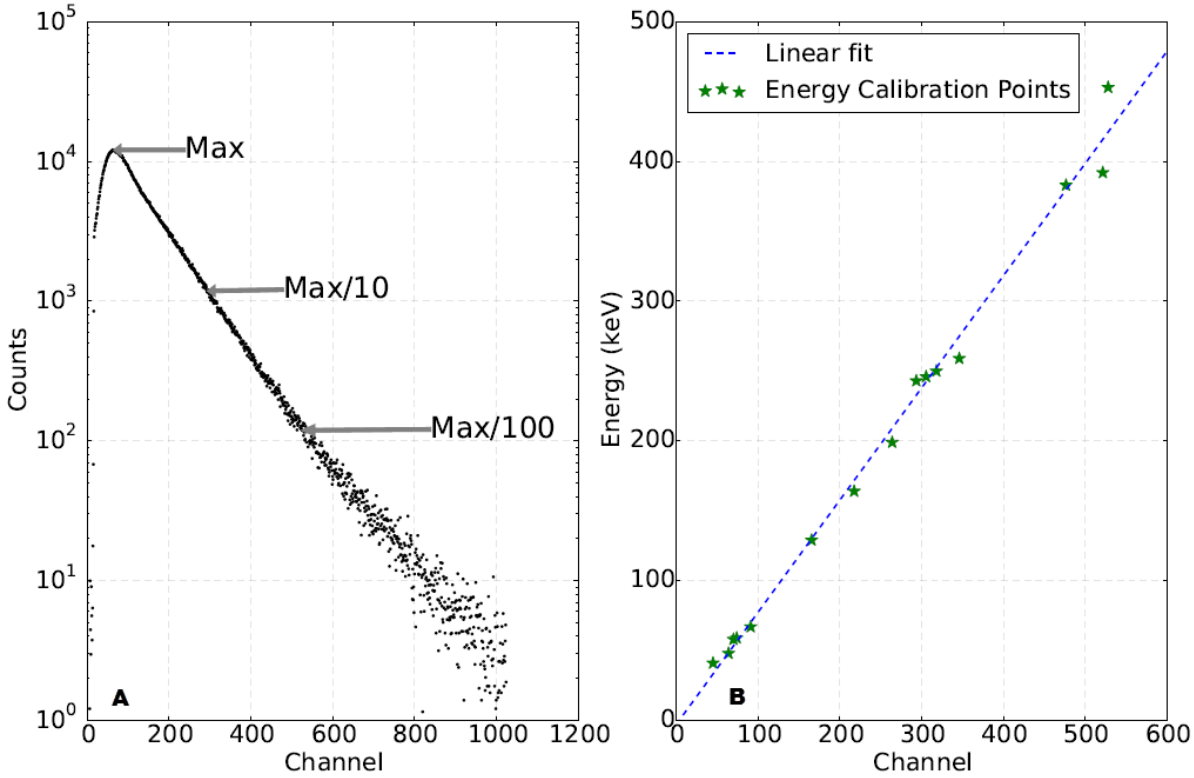

Fig. 3A and 3B. Sr/Y-90 pulse height spectrum (A) with the point of maximum, max/10 and max/100 counts marked. The corresponding channel numbers are then compared to the same points on a simulated spectrum and repeated for other nuclides. The corresponding coordinates are then plotted (B) and linear fit to determine the proper energy calibration for the detector.

Measurements with an energy calibrated MCA were made with point sources in close proximity to the surface of the detector as well as at a distance. The close proximity measurements were repeated at various locations on the large area scintillator, different positions relative to the PMT, and the result can be seen in Figure 4 where each hexagon corresponds to a hexagon formed by the frame of the detector, compare to Figure 2. The response relative to the center of the detector, directly at the collection end of the PMT, is given in the figure for both C-14 and Sr/Y-90. The C-14 response, top numbers, will be sensitive to both the dead layer thickness and light collection, while the Cl-36 response, bottom numbers, will be most affected by variations in light collection. The PMT is marked on this figure, and note that the response varies as a function of position, which is most likely due to varying degrees of light collection by the PMT. While only the response at the extreme locations are shown here, a more detailed mapping of the detector is found in [8]. The actual MCA output (with constant gain settings for each measurement) is shown in Figure 5 for three collection positions on the detector. Clearly the center of the detector, directly in front of the collection end of the PMT, shows the highest level of light output while opposite the PMT shows an average light output and behind the PMT shows a low light output. The average response of the probe is found both by exposing the entire detector to the beta field, when the source is

held at a distance, as well as with the source opposite the PMT. Furthermore, MCNP does not handle the light collection variations and this needs to be accounted for in another manner. Therefore, the position opposite the PMT was used to compare the MCNP model efficiency to the measured efficiency for all measurements made at the surface of the detector. This effect does create a source of uncertainty when dealing with very localized sources positioned very near to the detector face. This aspect is discussed later along with the complete uncertainty analysis.

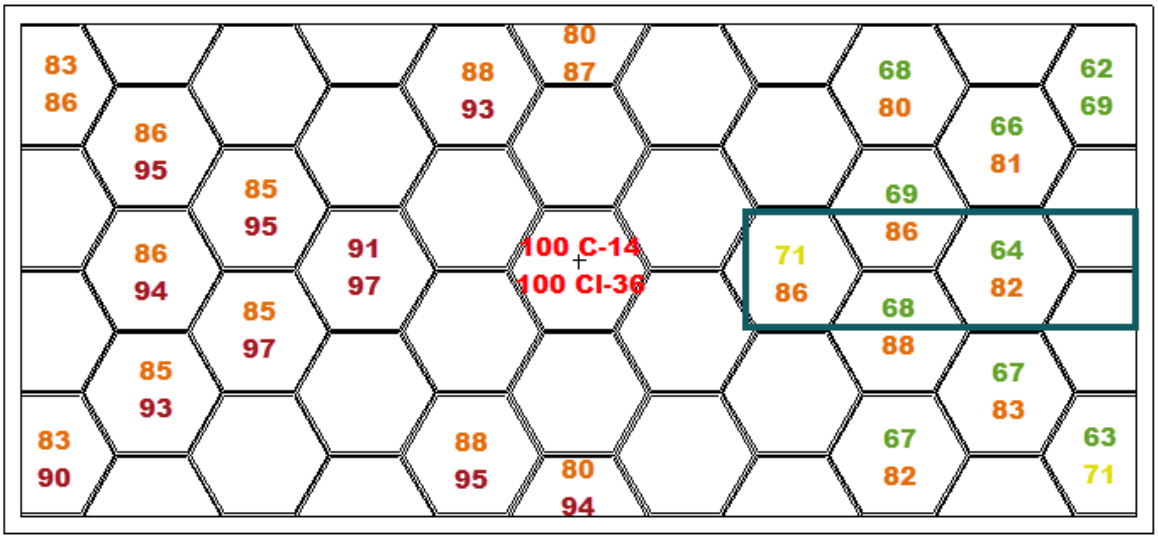

Fig. 4. Position dependent response for C-14 (top numbers at each position) and Cl-36 (bottom numbers for each position) given relative to the response at the center of the detector (in percent). The rectangle on the right of the image represents the placement of the PMT in the light pipe below the scintillator.

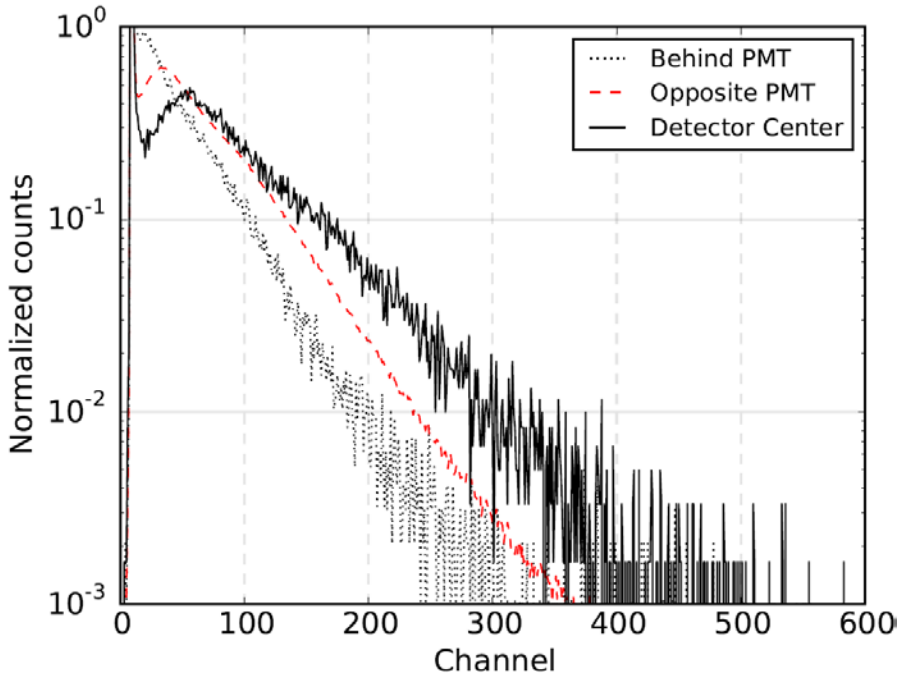

Fig. 5. Pulse height spectra for a Cl-36 point source at 3 positions on the detector. "Behind the PMT" corresponds to a point on the right of Figure 4, while "opposite PMT" corresponds to a position on the left of Figure 4.

Measurements were also made with various surface sources, 10cm x 10cm active area, placed both at the surface of the detector and at a distance. These geometries, both a surface source very close to the detector and at a distance, alleviate the uncertainty issue caused by light collection because a large portion of the detector is irradiated uniformly. The surface source measurements are also important because they test the MCNP model in a different range of entry angles across the detector than is done with point sources alone. In this geometry interactions with the protective Mylar layer as well as any detector dead layer will behave differently than with a point source. Furthermore, measurements at a distance will probe the models ability to deal with weakly absorbing media (the air) as well as the ability to predict the average response of the detector over a large area.

Finally, measurements were conducted with a Sr-90 surface source and a variety of HDPE absorbers between the source and the detector. Comparing these measurements to corresponding MCNP models test how the model is dealing with heavy absorption. If the model predicts heavy absorption correctly then it will likely predict the response to extended (volume) sources well also. These measurements simulate contributions to efficiency for various parts of a volumetric source, and when all contributions are integrated it provides an estimate of an infinitely thick source. That estimate can be compared directly to an MCNP model of a continuous extended volume source. From the discrete absorber layer source measurements we may arrive at an estimate of the continuous volume source by integrating over all absorber measurements. This was accomplished by using a

trapezoidal integration method on an energy bin by energy bin basis over the full set of measurements. The final outcome is a representation of the measured detector response to an extended volume source.

DISCUSSION

Monte Carlo Model Benchmark

The Monte Carlo model was benchmarked through a series of measurements with various nuclides including C-14, Tc-99, Cl-36, and Sr-90. These pure beta emitting nuclides range in maximum beta energy from 156 keV to 2280 keV and cover the typical range of expected beta energies. Furthermore, the benchmark included a mixed beta-gamma emitter ,Cs-137, for comparison as well. Measured spectra were compared for both shape and absolute efficiency to the modeled spectra for the cases of point sources, surface sources, and surface sources with absorbers.

The point source models show excellent agreement with the measurements across all nuclides. The shape of C-14 and Sr/Y-90 measured and modeled spectra are compared in Figures 6a and 6b respectively, where both nuclides show good shape agreement. Quantitative comparison for these nuclides as well as Tc-99 and Cl-36 are shown in TABLE I where the total efficiency from 60 keV to the max energy deposited is summed. Results show that the MCNP model is able to re-create the efficiency of the measured nuclides to within 12% over the range of beta emission energies. C-14 in particular with an average energy of 49 keV is highly sensitive to the thickness of a detector dead layer as well as the protective Mylar layer. Proper benchmark of this nuclide ensures that these parameters are correct. Sr/Y-90 on the other hand with the relatively high energy betas of Y-90, average energy 934 keV, provides a useful probe of the active detector thickness.

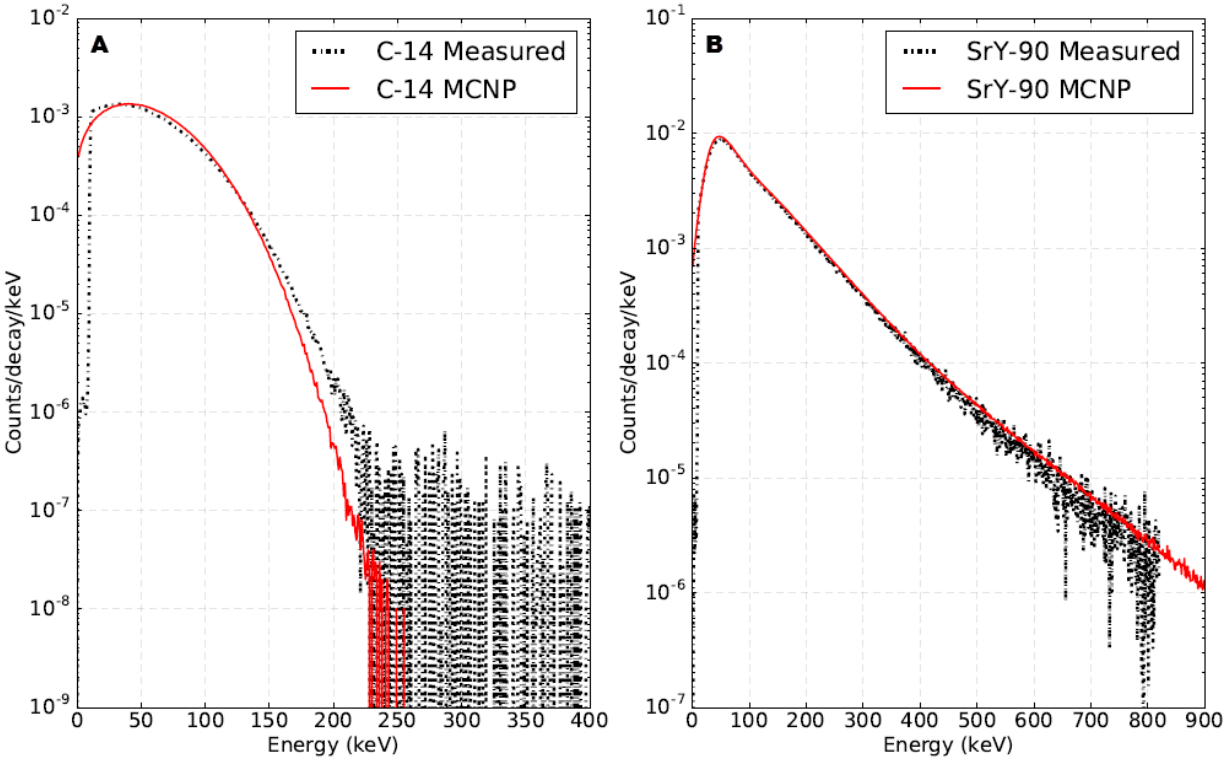

Fig. 6A and 6B. Measured and modeled point source spectra for C-14(A) and Sr/Y-90(B) at the surface of the detector.

TABLE I. Comparison of measured and modeled efficiency for various point sources

Nuclide	Counts / decay		MCNP / Measured	Source Uncertainty
	Measured	MCNP		
C-14	3.97E-02	4.44E-02	1.12	7.05%
Tc-99	1.58E-01	1.58E-01	1.00	3.22%
Cs-137	3.29E-01	3.39E-01	1.03	4.41%
Cl-36	3.64E-01	3.22E-01	0.89	3.91%
Sr-90	6.25E-01	6.54E-01	1.05	5.30%

The next logical step from a point source is to benchmark a surface source which contains activity distributed uniformly over two dimensions. Measurements were made with Sr/Y-90 and the comparison of the spectral shape to that of MCNP for each nuclide are shown in Figure 7a. Again, tabular data are also included, TABLE II, and show that agreement between the MCNP model and the measurement for the surface source without any absorber is within 5%. The MCNP model of the detector is now benchmarked for both point and surface sources.

Once the surface source geometry is benchmarked one may now investigate the effectiveness of the model to describe volume sources. One way to accomplish that is to first measure/model the surface source with various thickness of absorber

between the source and the detector. Starting from no absorber up to an absorber that completely stops all beta particles from reaching the detector, each geometry represents a different layer of an infinitely thick source. It is then possible to integrate over the various layers to arrive at a representation of the infinitely thick source. The process of integrating the various layers can be conducted for both the measurements and the MCNP models. Furthermore, an MCNP model of the actual infinitely thick source that the integration represents can also be produced for comparison.

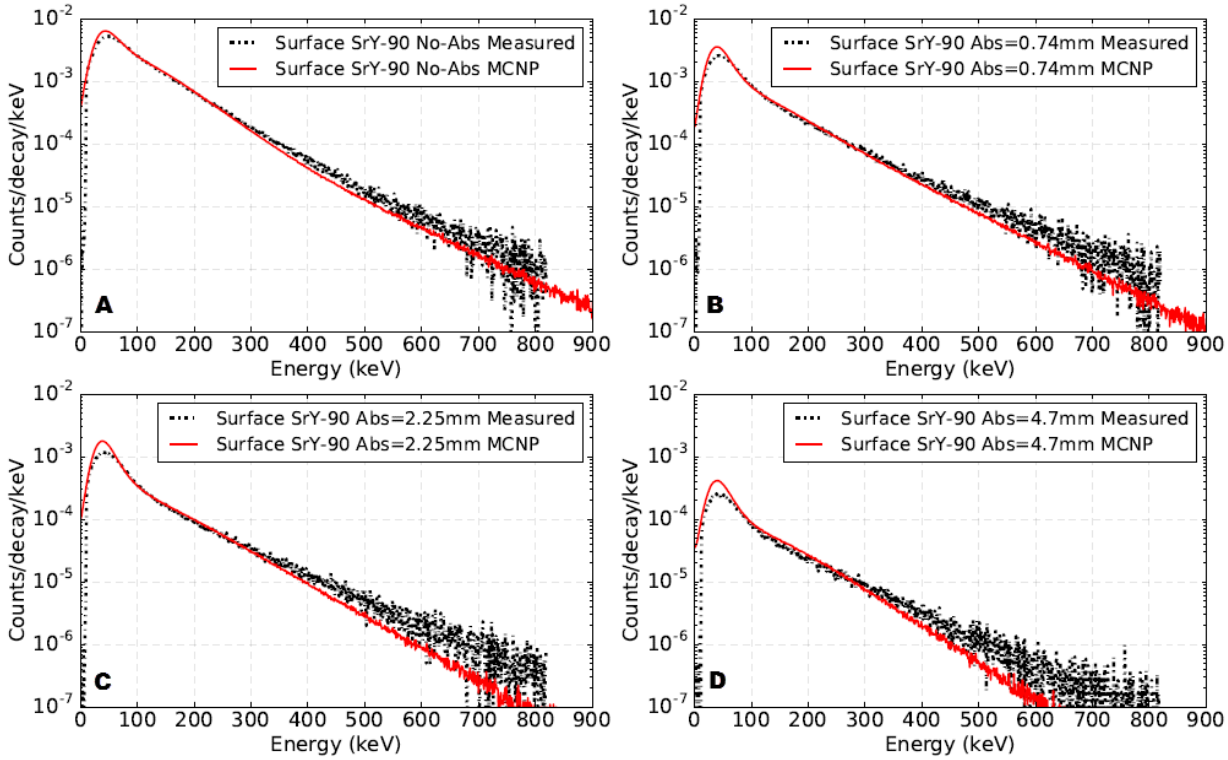

Fig. 7A, 7B, 7C, and 7D. Comparison of measured and modeled pulse height spectra for a Sr/Y-90 surface source at 44 mm with various HDPE absorbers between the source and the detector.

TABLE II. Comparison of measured to modeled efficiencies for a Sr/Y-90 surface source with various HDPE absorbers

Absorber Thickness (mm)	Counts / decay		MCNP / Measured	Source uncertainty
	Measured	MCNP		
None	3.36E-01	3.40E-01	1.01	5.83%
0.74	1.20E-01	1.20E-01	1.00	5.83%
0.74	1.19E-01	1.20E-01	1.01	5.83%
1.68	6.82E-02	6.83E-02	1.00	5.83%
2.25	5.13E-02	5.16E-02	1.01	5.83%

3.17	3.10E-02	3.24E-02	1.05	5.83%
4.7	1.19E-02	1.34E-02	1.12	5.83%
6.22	3.26E-03	4.37E-03	1.34	5.83%
9.46	-3.71E-04	6.10E-05	-0.16	5.83%

The infinitely thick benchmark starts with the comparison of the measured and modeled surface source with various layers of absorber. These are displayed graphically for shape and in tabular for quantitative comparison in Figure 7 and TABLE II respectively. Note that the agreement is within 5% for absorbers up to 3.17 mm thick and then agreement deteriorates as the absorber grows thicker. However, since a very large portion of the efficiency of a volumetric source, 98%, originates from the first 3.17 mm of the source, the disagreement at very thick absorber values will have little effect on the efficiency of an infinitely thick source.

Once the series of absorber measurements and models are integrated over the total thickness of the thickest absorber, they may then also be compared for shape and total efficiency. The integrated, measured and modeled, spectra and modeled infinitely thick spectra are compared in Figure 8 while the data are compared quantitatively in TABLE III. We see agreement within 5% for this geometry when the 60 keV LLD is used, which now benchmarks the MCNP model for 3 dimensional sources. The 60 keV has been chosen in general throughout the analysis because at this point the spectrum is free from any possible electronic noise as well as any adverse effects during elevated count rates.

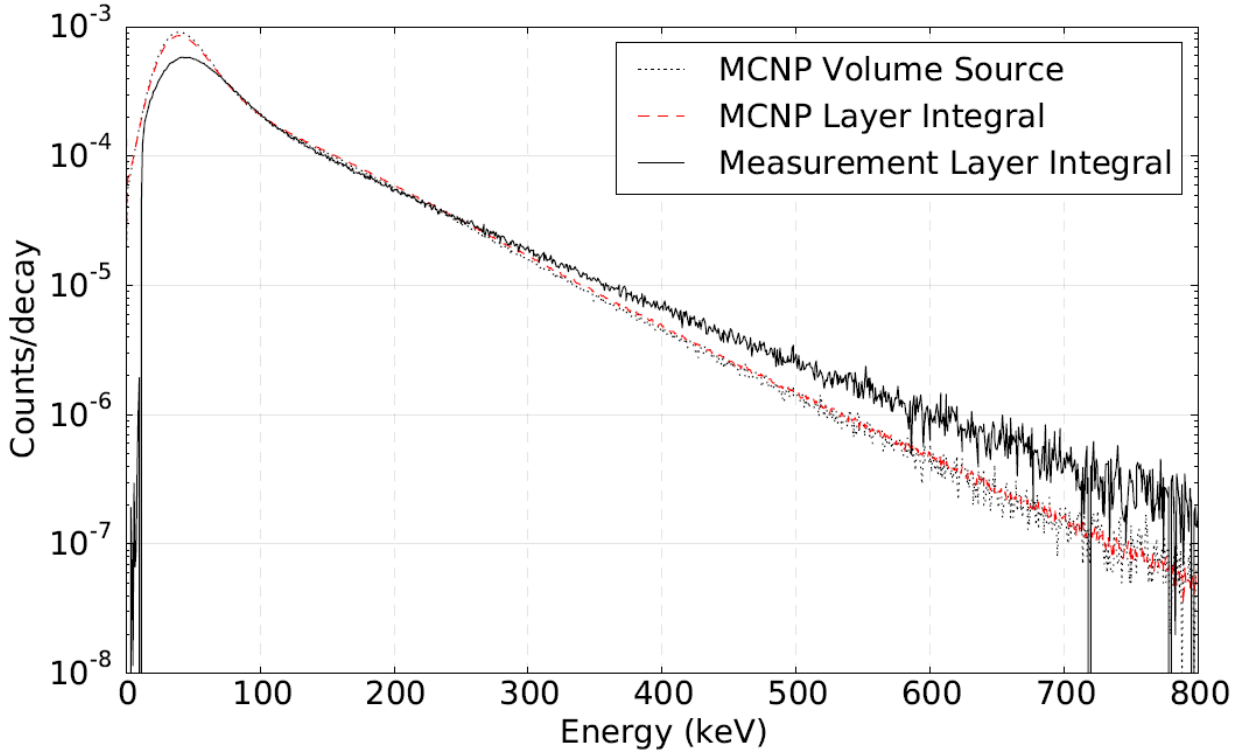

Fig. 8. Comparison of MCNP simulation of a volume source with an integrated

spectrum formed by integrating the detector response to measurements made with varying absorber thickness. The integration technique was also tested on exact MCNP models of the various measurement geometries.

TABLE III. Comparison of efficiency for the volume source based on a volumetric MCNP model, integrated measurements with various absorbers, and integrated MCNP models with various absorbers.

LLD (keV)	MCNP Volume	Meas. Integral	MCNP Integral	Meas./MCNP Volume	Meas./MCNP Integral	MCNP Integral/ MCNP Volume
20	7.56E-02	6.27E-02	7.41E-02	0.83	0.85	0.98
60	3.76E-02	3.74E-02	3.82E-02	1.00	0.98	1.02

Uncertainty analysis

While counting statistics did not play a major role in the uncertainty budget with the exception of measurements made with ~1cm thick HPDE absorbers, other contributors to the uncertainty include the individual source activities, positioning uncertainty, choice of LLD, and for the volumetric comparison differences between the multiple measured spectra and the single infinitely thick MCNP geometry. Finally, there is a contribution to the measurement uncertainty that depends on the location of activity relative to the surface of the detector. Activity directly above the collection end of the PMT corresponds to a larger signal than activity behind the opening of the PMT. Therefore, the efficiency of a given nuclide is slightly position dependent when the source is very localized. This effect is alleviated by choosing the average response position opposite the PMT when conducting measurements at the surface of the detector. For the surface sources or for measurements at a distance this effect was not an issue. A blanket uncertainty of 3% was given to all measurements to account for this effect.

With respect to the absorber measurements compared to the single infinite thickness model there are a few issues that contribute to uncertainty. First, the surface source measurements with absorbers were all conducted with the source at a fixed location relative to the detector (44m). During the measurement process various thicknesses of HDPE absorber were inserted between the detector and the source, but the source to detector distance remained unchanged. However, when an extended MCNP model of the volumetric source is produced, the active source material is found at a continuum of distances from the detector ranging from the front surface of the source to the back surface of the source. Therefore, an estimate distance scale factor must be applied to compare the results. The uncertainty associated with this effect was estimated as an additional 2% uncertainty in the overall positioning uncertainty.

The full uncertainty budget for measurements with each source is given in TABLE IV. Note that counting statistics are not a significant source of uncertainty for any of the measurements with the exception of the 9.46 mm thick absorber measurement, which was omitted from the table.

Table IV. Uncertainty budget for each measurement geometry. All uncertainties are quoted at 1 sigma. Counting statistics are not a significant source of uncertainty.

Geometry	Nuclide	Activity (%)	Position (%)	LLD/Energy cal (%)	Total 1 sigma (%)
Point	C-14	2.35	3	3	4.85
Point	Tc-99	1.07	3	3	4.38
Point	Cl-36	1.30	3	3	4.44
Point	Cs-137	1.47	3	3	4.49
Point	Sr/Y-90	1.77	3	3	4.60
Surface	Sr/Y-90	1.94	3	3	4.67
Surface Abs	Sr/Y-90	1.94	3	3	4.67
Infinite	Sr/Y-90	1.94	5	3	6.15

Applications

A benchmarked MCNP model of the TPS-B probe allows for rapid prototyping of systems for various purposes including emergency response. The benchmark allows confidence at better than the 20% level for geometries including points and surfaces as well as sources with extended thickness and even infinitely thick source geometries. A specific application where MCNP modeling of the TPS-B detector was utilized is a Sr-90 water monitor [9] for the Fukushima cleanup effort. In this case modeling was performed to optimize the sensitivity a system to beta radiation from Sr/Y-90 while minimizing the sensitivity for gamma and other lower energy beta emitters. With the benchmarked model in hand it is now possible to fine tune the monitor dimensions to optimize performance for various beta emitting nuclides. Similarly, the benchmarked model could be used to rapidly determine the performance of and produce conveyor based dirt, log, or object monitors. Other areas of opportunity include improving performance of portal and personnel monitors that already use the detectors.

CONCLUSION

Monte Carlo models of thin plastic scintillator based beta detectors have been produced and vigorously validated. Verification measurements included point sources, surface sources, surface sources with varying thickness absorbers, and extended volume sources. The results show agreement within 12% for point sources of various nuclides close to the detector, 5% for surface sources with HDPE absorbers from 0 to 3.17 mm, and within 5% for volume sources. With a properly benchmarked model in hand, rapid prototyping and nuclide specific efficiencies may be produced for systems based on the TPS-B detector. Future work will include similar characterization of other detectors in the TPS family such as the TPS-BG (beta-gamma dual scintillator), TPS-AB (alpha-beta dual scintillator), and the Zeus

(gamma scintillator)

REFERENCES

1. E. R. Siciliano *et al.,* "Comparison of PVT and NaI(Tl) scintillators for vehicle portal monitor applications", Nuclear Inst. and Methods in Physics Research, A, **550**, 647-674 (2005)
2. K. Chankyu *et al.*, "Iterative Monte Carlo simulation with the Compton kinematics-based GEB in a plastic scintillator detector", Nuclear Inst. And Methods in Physics Research, A , **795**, 298-304 (2015)
3. S. Ashrafi and S. M. Etesami, "Monte Carlo simulation of a plastic scintillator response function in beta-gamma coincidence measurement", Radiation Measurements, **43(9-10),** 1511-1514 (2008)
4. S. Kwak *et al.*, "Plastic scintillator-based radiation detector for mobile radiation detection system against nuclear/radiological terrorism", Nuclear Inst. And Methods in Physics Research, A, **604**, 161-163 (2009)
5. G. F. Knoll, "Radiation Detection and Measurement", Third Ed., Wiley, New York, New York (2000)
6. X-5 Monte Carlo Team, "MCNP – A general Monte Carlo N Particle Transport Code Version 5", Los Alamos national Laboratory Report LA-UR-03-1987 (2003)
7. A. N. Berlizov, "MCNP-CP Manual, A Correlated Particle Source Extension of a General Purpose Monte Carlo N-Particle Transport Code", User's Manual Version 02 (2006)
8. K. K. Pourtangestani, "Optimization of Plastic Scintillator Thickness for Online Beta Detection in Mixed Fields", Master of Science Thesis, University of Ontario Institute of Technology (2010)
9. J. K. Zickefoose *et al.*, "Performance of a low activity beta-sensitive Sr-90 water monitor", Journal of Radioanalytical and Nuclear Chemistry, **307(3)**, 1819-1824 (2016)